dmj
DIABETES & METABOLISM JOURNAL

PDZD8 Augments Endoplasmic Reticulum-Mitochondria Contact and Regulates Ca^{2+} Dynamics and Cypd Expression to Induce Pancreatic β-Cell Death during Diabetes

Yongxin Liu, Yongqing Wei, Xiaolong Jin, Hongyu Cai, Qianqian Chen, Xiujuan Zhang

Diabetes Metab J 2024;48:1058-1072 | https://doi.org/10.4093/dmj.2023.0275

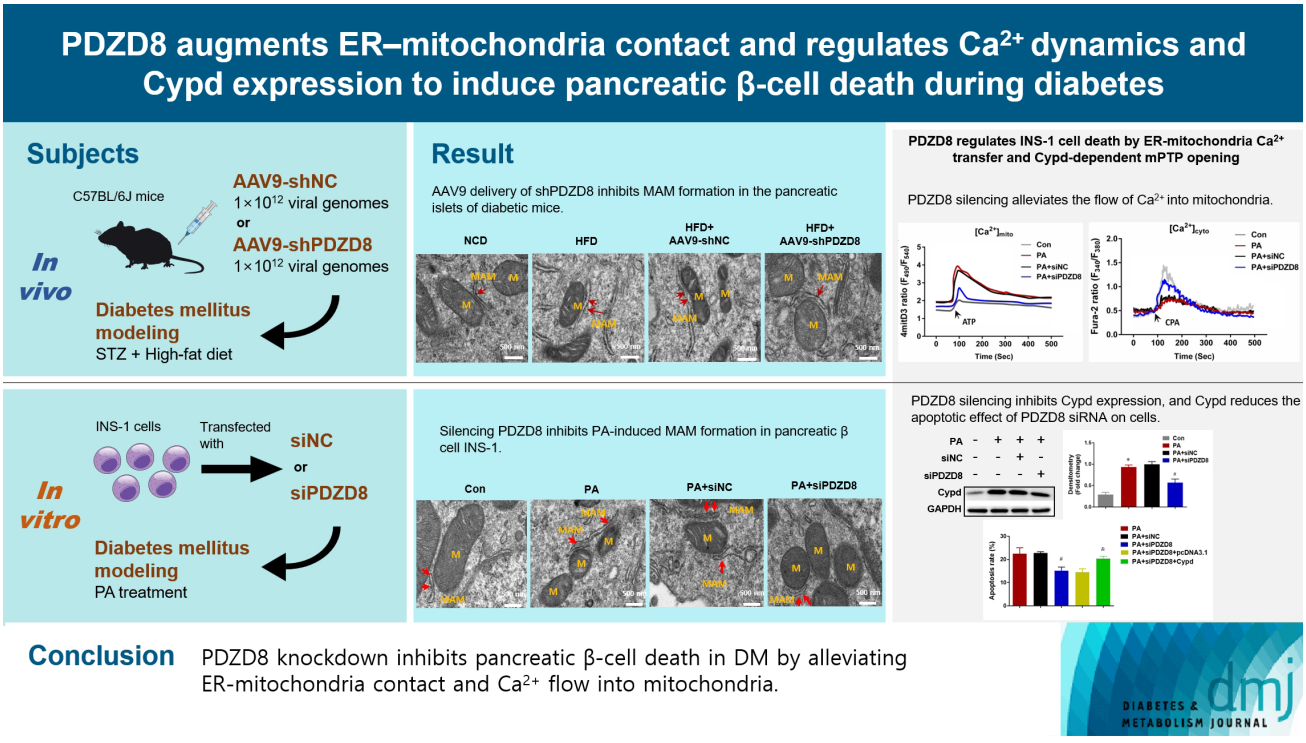

Highlights

- **HFD-induced diabetes shows MAM formation and PDZD8 expression in islets.**
- **Knockdown of PDZD8 inhibits MAM formation in islets and pancreatic β-cells.**
- **PDZD8 knockdown reduces mitochondrial dysfunction in pancreatic β-cells.**
- **PDZD8 controls ER-mitochondria Ca^{2+} transfer and mPTP opening in pancreatic β-cells.**

How to cite this article:
Liu Y, Wei Y, Jin X, Cai H, Chen Q, Zhang X. PDZD8 Augments Endoplasmic Reticulum-Mitochondria Contact and Regulates Ca^{2+} Dynamics. and Cypd Expression to Induce Pancreatic β-Cell Death during Diabetes. Diabetes Metab J 2024;48:1058-1072. https://doi.org/10.4093/dmj.2023.0275

Original Article
Basic Research

Diabetes Metab J 2024;48:1058-1072
https://doi.org/10.4093/dmj.2023.0275
pISSN 2233-6079 · eISSN 2233-6087

dmj
DIABETES & METABOLISM JOURNAL

PDZD8 Augments Endoplasmic Reticulum-Mitochondria Contact and Regulates Ca^{2+} Dynamics and Cypd Expression to Induce Pancreatic β-Cell Death during Diabetes

Yongxin Liu[1,*], Yongqing Wei[2,*], Xiaolong Jin[3], Hongyu Cai[3], Qianqian Chen[3], Xiujuan Zhang[1,3]

[1]Department of Endocrinology, Shandong Provincial Hospital, Shandong University, Jinan,
[2]Department of Obstetrics, Central Hospital Affiliated to Shandong First Medical University, Jinan,
[3]Department of Endocrinology, Shandong Provincial Hospital Affiliated to Shandong First Medical University, Jinan, China

Background: Diabetes mellitus (DM) is a chronic metabolic disease that poses serious threats to human physical and mental health worldwide. The PDZ domain-containing 8 (PDZD8) protein mediates mitochondria-associated endoplasmic reticulum (ER) membrane (MAM) formation in mammals. We explored the role of PDZD8 in DM and investigated its potential mechanism of action.
Methods: High-fat diet (HFD)- and streptozotocin-induced mouse DM and palmitic acid (PA)-induced insulin 1 (INS-1) cell models were constructed. PDZD8 expression was detected using immunohistochemistry, quantitative real-time polymerase chain reaction (qRT-PCR), and Western blotting. MAM formation, interactions between voltage-dependent anion-selective channel 1 (VDAC1) and inositol 1,4,5-triphosphate receptor type 1 (IP3R1), pancreatic β-cell apoptosis and proliferation were detected using transmission electron microscopy (TEM), proximity ligation assay (PLA), terminal deoxynucleotidyl transferase dUTP nick end labeling (TUNEL) assay, immunofluorescence staining, and Western blotting. The mitochondrial membrane potential, cell apoptosis, cytotoxicity, and subcellular Ca^{2+} localization in INS-1 cells were detected using a JC-1 probe, flow cytometry, and an lactate dehydrogenase kit.
Results: PDZD8 expression was up-regulated in the islets of HFD mice and PA-treated pancreatic β-cells. PDZD8 knockdown markedly shortened MAM perimeter, suppressed the expression of MAM-related proteins IP3R1, glucose-regulated protein 75 (GRP75), and VDAC1, inhibited the interaction between VDAC1 and IP3R1, alleviated mitochondrial dysfunction and ER stress, reduced the expression of ER stress-related proteins, and decreased apoptosis while increased proliferation of pancreatic β-cells. Additionally, PDZD8 knockdown alleviated Ca^{2+} flow into the mitochondria and decreased cyclophilin D (Cypd) expression. Cypd overexpression alleviated the promoting effect of PDZD8 knockdown on the apoptosis of β-cells.
Conclusion: PDZD8 knockdown inhibited pancreatic β-cell death in DM by alleviated ER-mitochondria contact and the flow of Ca^{2+} into the mitochondria.

Keywords: Diabetes mellitus; Endoplasmic reticulum; Mitochondria; Pdzd8 protein, mouse

INTRODUCTION

Diabetes mellitus (DM) is a chronic metabolic disease that is a major global threat to human physical and mental health [1]. Type 2 diabetes mellitus (T2DM) accounts for approximately 90% of all diagnosed cases with diabetes [2,3]. Insulin resis-

Corresponding author: Xiujuan Zhang https://orcid.org/0009-0001-5959-7652
Department of Endocrinology, Shandong Provincial Hospital, Shandong University, No. 324, Huaiyin District, Shandong, P.R. Jinan 250000, China
E-mail: zhangxiujuan@sdfmu.edu.cn

*Yongxin Liu and Yongqing Wei contributed equally to this study as first authors.

Received: Aug. 12, 2023; Accepted: Mar. 26, 2024

tance and pancreatic β-cell dysfunction are the major features of T2DM [4]. Maintaining β-cell mass and protecting against β-cell dysfunction may be effective measures to alleviate T2DM.

The endoplasmic reticulum (ER) and mitochondria control vital biological processes, including cell metabolism, energy production, calcium homeostasis, and protein synthesis [5]. Under many pathological conditions, ER is usually related toxidative stress, metabolic defects, and mitochondrial damage [6,7]. The mitochondria and ER are interconnected organelles, and their contact sites are called mitochondria-associated ER membranes (MAMs) [8,9]. The physical interactions at MAM simply that ER stress and mitochondrial dysfunction usually co-exist [10]. Moreover, the ER and mitochondria are key metabolic organelles for β-cell function. ER activation plays a crucial role in insulin response to glucose synthesis, proper folding, and classification. The ER forms a major intracellular Ca^{2+} reservoir, and the controlled release of Ca^{2+} into cytosol is an essential step in insulin synthesis [11]. Under normal circumstances, low constitutive levels of calcium are released from the ER to maintain calcium signaling and adenosine triphosphate (ATP) production in the mitochondria [12,13]. Nevertheless, the role of MAM in pancreatic β-cell dysfunction needs further investigation.

PDZ domain-containing 8 (PDZD8) is a recently identified protein that mediates the formation of the mammalian MAM [14]. It contains a synaptic-binding protein-like mitochondrial lipid-binding domain and is involved in binding these membrane contact sites through interactions with many proteins and membrane lipids [15]. PDZD8 forms complexes with protrudin, VAMP-associated protein (VAP), and member RAS oncogene family (Rab7) at membrane contact sites between the ER and late endosomes and lysosomes (LES/Lys) to regulate the transfer of lipids from ER to LES/Lys [16-19]. Studies have shown that PDZD8 promotes the progression of lung adenocarcinoma and gastric cancer [20,21]. Additionally, PDZD8 is involved in cytoskeletal modulation as a moesin-interacting protein [22]. However, whether PDZD8 is involved in the regulation of pancreatic β-cell function remains unclear.

In this study, we established a diabetic mouse model and a cell model to detect PDZD8 expression and function in pancreatic β-cells. The MAM perimeter and MAM-related protein expression, voltage-dependent anion-selective channel 1 (VDAC1)–inositol 1,4,5-triphosphate receptor type 1 (IP3R1) interaction, mitochondrial membrane function, and ER stress-related protein expression in islet tissues and pancreatic β-cells were explored. Additionally, the mitochondrial Ca^{2+} level and cyclophilin D (Cypd) protein expression in β-cells were detected. Our findings suggest that PDZD8 induces death in pancreatic β-cells in DM by enhancing ER-mitochondrial contact and regulating Ca^{2+} kinetics and Cypd expression.

METHODS

DM animal model

C57BL/6J mice (male, 8-week-old, Jinan Pengyue Experimental Animal Breeding Co. Ltd., Jinan, China) were divided into a normocaloric diet (NCD) group ($n=6$) and a high-fat diet (HFD) group ($n=24$). The experimental protocol was performed in accordance with the Guide for the Care and Use of Laboratory Animals and was protocol approved by the Shandong Provincial Hospital (approve no.: 2022-283).

The model group was fed HFD for 12 weeks and then fasted for 6 hours. After fasting, a 1% streptozotocin (STZ; Yeasen, Shanghai, China) solution was injected intraperitoneally at a dose of 30 mg/kg body weight for 7 consecutive days. After STZ injection, blood samples were collected from the tail vein to determine fasting blood-glucose levels. Mice with a fasting blood-glucose ≥11.1 mmol/L were formally included in the HFD group ($n=18$). After screening, the mice continued to be fed HFD for 12 weeks. Finally, the mice were anaesthetized with a 2% pentobarbital sodium injection, the pancreas was excised, blood was collected, and the serum was centrifuged for subsequent experiments.

AAV9 delivery of shPDZD8

Two weeks before STZ injection, 12 of the HFD mice were administrated with either adeno-associated virus 9 (AAV9)-shRNA negative control (shNC) (AAV9-shNC group; $n=6$) or AAV9-short hairpin PDZD8 (shPDZD8) (AAV9-shPDZD8 group; $n=6$) at a dose of 1×10^{12} viral genomes per mouse via tail vein injection.

Transmission electron microscopy

Islet tissues and insulin 1 (INS-1) cells were fixed with 2.5% glutaraldehyde for 2 hours, stained with 1% osmium tetroxide for 1 hour, dehydrated in ethanol, and then treated with propylene oxide. After embedding in Epon 812 epoxy resin, the tissues and cells were sectioned into 100-nm ultrathin sections. After staining with uranyl acetate and lead citrate, the results were observed using a Bio-HVEM system (JEOL, Akishima,

Japan). The perimeters of MAM and mitochondria were measured using the ImageJ software (National Institutes of Health, Bethesda, MD, USA).

Immunohistochemistry

The pancreatic tissue was fixed in 4% formaldehyde, and then dehydrated, vitrified, waxed, embedded and sliced into sections. After incubation with anti-PDZD8 antibody (bs-9043R; Bioss Antibodies, Woburn, MA, USA) at 4°C overnight, the sections were incubated with horseradish peroxidase (HRP)-labeled secondary antibody (31460; Thermo Fisher Scientific, Shanghai, China) at 25°C for 60 minutes. The sections were stained with 3,3′-diaminobenzidine tetrahydrochloride hydrate (DAB) color-developing solution (P0202; Beyotime, Shanghai, China) and hematoxylin. Staining results were observed and photographed under a light microscope.

Proximity ligation assay

The islet tissue was subjected to antigen extraction and peroxidase quenching according to the immunohistochemical description. INS-1 cells were fixed with 4% paraformaldehyde and vitrified using 0.2% Triton-X. The sections and cells were incubated with primary antibodies (VDAC1, ab186321 and IP3R1, ab308165; both from Abcam, Cambridge, UK) at 4°C overnight and secondary antibody conjugated with anti-rabbit proximity ligation assay (PLA) probe Plus (DUO92002; Merck, Shanghai, China) and anti-mouse PLA probe Minus (DUO92004; Merck) at 37°C for 1 hour. Images were captured under a light or fluorescence microscope.

Assessment of mitochondrial function

The islet tissues were minced into small pieces and rinsed in ice-cold phosphate buffer saline (PBS) to thoroughly remove excess blood. The tissues were then homogenized in PBS with a glass homogenizer on ice. The homogenates were centrifuged for 5 minutes at 5,000 ×*g* to obtain the supernatant and stored at –20°C.

(1) Hydrogen peroxide (H_2O_2) detection: H_2O_2 production in the islet tissues was detected using the Amplex Red Hydrogen Peroxide/Peroxidase Assay Kit (A22188; Thermo Fisher Scientific). The supernatant was mixed with 50 μL of 10 mM Amplex Red reagent stock solution, 100 μL of 10 U/mL HRP stock solution, and 4.85 mL of 1X Reaction Buffer and then incubated at room temperature for 30 minutes. The absorbance at 570 nm was measured using a spectrophotometer, and H_2O_2 production was calculated using a standard curve.

(2) Lipid peroxidation analysis: the lipid peroxidation analysis was detected using the competition enzyme-linked immunosorbent assay (ELISA) kit for 4-hydroxynonenal (ABIN6964478; Antibodies-online, Aachen, Germany). The 96-well plates were washed two times before adding the samples. The samples (50 μL) and biotin-labeled antibody (50 μL) were added into each well, mixed thoroughly and then incubated at 37°C for 45 minutes. The plates were washed three times with Wash Buffer. HRP-streptavidin conjugate working solution (100 μL) was added into each well and incubated at 37°C for 30 minutes. After washing the plates five times with wash buffer, 3,3′,5,5′-tetramethylbenzidine (TMB) substrate (90 μL) was added into each well and incubated at 37°C in the dark within 15 minutes. Stop solution (50 μL) was then added into each well and the absorbance at 450 nm was immediately read using a microplate reader.

(3) The ATP levels in the mitochondria of the islet tissues were detected using the ATP assay kit (ab83355; Abcam). The plates were set up for standard (50 μL), samples (50 μL), and sample background controls (50 μL). After preparation, ATP reaction mix (50 μL) was added to each standard and sample well, and background reaction mix (50 μL) was added to the sample background control wells. The plates were incubated at 25°C for 30 minutes in the dark, and the fluorescence intensity at Ex/Em=535/587 nm was measured.

(4) Mitochondrial DNA (mtDNA) quantification: mtDNA and genomic DNA were isolated from the islet tissues and INS-1 cells using the DNeasy Blood & Tissue Kit (69506; Qiagen, Shanghai, China). mtDNA was quantified using quantitative real-time polymerase chain reaction (qRT-PCR).

TUNEL staining

The apoptosis of β-cells in islets was detected using the terminal deoxynucleotidyl transferase dUTP nick end labeling (TUNEL) apoptosis assay kit (C1091; Beyotime). After dewaxing and hydration, the sections were incubated with protease K solution at 25°C for 15 minutes to remove tissue protein. To inactivate the endogenous peroxidase, the sections were incubated in 3% H_2O_2 at 25°C for 20 minutes. After PBS washing, the sections were incubated with 50 μL biotin-labeling solution at 37°C in dark for 1 hour and 0.5 mL DAB color-developing solution at 25°C for 30 minutes. Images were captured under a light microscope.

Immunofluorescent staining

The pancreatic tissue was fixed in 4% formaldehyde, dehydrated in 30% sucrose, and embedded in optimal cutting temperature compound. Tissues were sectioned into 5-μm thick and incubated with primary anti-insulin (#3014, Cell Signaling Technology, Danvers, MA, USA) or anti-Ki67 (27309-1-AP, Proteintech, Rosemont, IL, USA) antibodies at 4°C overnight followed by incubation with anti-rabbit immunoglobulin G (IgG) secondary antibodies (#4413 or #4412, Cell Signaling Technology) at room temperature for 1 hour. Nuclei were stained with 4′,6-diamidino-2-phenylindole (DAPI). The sections were photographed under a fluorescence microscope.

Pancreatic β-cell culture

INS-1 cells (Procell, Wuhan, China) were cultured in RPMI-1640 containing 10% fetal bovine serum, 50 μmol/L β-mercaptoethanol, and 1% penicillin–streptomycin solution (Procell) at 37°C. Palmitic acid (PA; S30037, Shanghai YuanyeBio-Technology Co. Ltd., Shanghai, China) dissolved in dimethyl sulfoxide (DMSO) was used to treat cells at a dose of 0.5 mM for 24 hours.

Cell transfection

The siRNA PDZ domain-containing 8 (siPDZD8; 5′-GCTTAAAGTTACATTGCTAGA-3′), negative control (siNC; 5′-GCATATTAAGTAGTCGTTACA-3′), Cypd overexpressed plasmid (Cypd), and the empty pcDNA3.1 vector (pcDNA3.1) were purchased from RiboBio (Guangzhou, China). Lipofectamine 3000 was used for INS-1 cell transfection for 48 hours according to the manufacturer's instructions.

Apoptosis detection

INS-1 cells were collected, resuspended with 1× binding buffer, and mixed with Annexin V/FITC (CA1020, Solarbio, Beijing, China) in a flow tube and incubated at 25°C for 5 minutes in the dark. After adding propidium iodide solution and PBS to the flow tube, flow detection was performed immediately.

Lactate dehydrogenase assay

INS-1 cells were cultured in 96-well plates (5×10^3 cells/well) for 24 hours and then incubated with lactate dehydrogenase (LDH) release reagent (C0016; Beyotime) at 37°C for 1 hour. LDH release was quantified by measuring the absorbance at 490 nm using a microplate reader (Thermo Fisher Scientific).

Glucose-stimulated insulin secretion

INS-1 cells were pre-incubated with Krebs-Ringer Buffer (KRB; G0430, Solarbio) containing 2.8 mM of glucose for 2 hours and incubated with KRB containing 2.8 or 16.7 mM of glucose for 1 hour at 37°C. Insulin secretion in the media was measured using an insulin ELISA kit (E-EL-R2466c, Elabscience, Houston, TX, USA).

qRT-PCR

Total RNA was extracted from islet tissues using TRIzol (R0016, Beyotime). The first-strand cDNA synthesis kit (D7168, Beyotime) was used to synthesize first-strand cDNA. Quantitative polymerase chain reaction (qPCR) was performed using Cham QSYBR qPCR Master Mix (Q311, Vazyme, Nanjing, China). mRNA levels were calculated using the $2^{-\Delta\Delta Ct}$ method. The primer sequences were as follows: PDZD8, 5′-GCTCATTGCTATTGGAGGTGTG-3′ (F) and 5′-AGCTTTCTTCCAACTGGCCC-3′ (R); β-actin, 5′-CACTGTCGAGTCGCGTCC-3′ (F) and 5′-TCATCCATGGCGAACTGGTG-3′ (R).

Western blotting

Total protein was isolated from the tissues and cells using radio-immunoprecipitation assay (RIPA) buffer (P0013C, Beyotime). The protein samples were separated using 10% sodium dodecyl sulfate–polyacrylamide gel electrophoresis and then transferred onto polyvinylidene fluoride membranes. The membranes were blocked with non-fat milk for 2 hours. After incubation with primary antibodies at 4°C overnight, the membranes were incubated with secondary antibody for 2 hours at 25°C. The bands were visualized using an enhanced chemiluminescent kit (P0018, Beyotime). The primary antibodies were PDZD8 (bs-9043R, Bioss Antibodies), IP3R1 (ab308165, Abcam), glucose-regulated protein 75 (GRP75; 14887-1-AP, Proteintech), VDAC1 (ab186321, Abcam), protein disulfide isomerase (#3501, Cell Signaling Technology), cytochrome c oxidase 4 (COX IV; #4850, Cell Signaling Technology), β-tubulin (10094-1-AP, Proteintech), protein kinase R (PKR)-like endoplasmic reticulum kinase (PERK; ab229912, Abcam), phosphorylated PERK (p-PERK; PA5-40294, Thermo Fisher Scientific), eukaryotic translation initiation factor 2A (eIF2α; #5324, Cell Signaling Technology), p-eIF2α (#3597, Cell Signaling Technology), activating transcription factor 4 (ATF4; 60035-1-Ig, Proteintech), C/EBP-homologous protein (CHOP; 15204-1-AP, Proteintech), glyceraldehyde 3-phosphate dehydrogenase (ab9485, Abcam), BCL2 associated X,

apoptosis regulator (Bax; 50599-2-Ig, Proteintech), B cell lymphoma 2 (Bcl-2; ab196495, Abcam), cleaved caspase3 (19677-1-AP, Proteintech), and Cypd (ab231155, Abcam). The secondary antibody was goat anti-rabbit/mouse IgG H&L (HRP) (ab6721 or ab6789, respectively; Abcam).

Mitochondrial membrane potential detection

The mitochondrial membrane potential was measured using a mitochondrial membrane potential assay kit with JC-1 (C2006, Beyotime). INS-1 cells were seeded into 6-well plate (5×10^5 cells/well) and cultured for 12 hours. Cells were incubated with JC-1 staining working solution at 37°C for 20 minutes. The supernatant was removed and the cells were washed twice with JC-1 dye buffer. After resuspending the cells in cell culture medium, the results were observed under a fluorescence microscope. For imaging the JC-1 monomer, the excitation wavelength was 490 nm and the emission wave length, 530 nm; for JC-1 aggregates, the excitation wave length was 525 nm and the emission wavelength, 590 nm.

Subcellular Ca^{2+} measurement

INS-1 cells were cultured with Fura-2 AM (40702ES50, Yeasen) on coverslips and then washed with Ca^{2+}-free KRB (G0430, Solarbio). After transfer to the perfusion chamber under an inverted microscope (Olympus, Tokyo, Japan), the cells were alternately excited at 340 and 380 nm using a monochromatic light source (LAMDA DG-4, Sutter, Novato, CA, USA). The fluorescence images were photographed at 510 nm with an intensified CCD camera (Roper Scientific, Trenton, NJ, USA). The fluorescence intensity ratio (F340/F380) was estimated using the MetaFluor 6.1 software (Molecular Devices Corp., Downington, PA, USA). The Ca^{2+} levels in the mitochondria and cytoplasm were measured with protein probe Fura-2. The cells were excited at wavelengths of 540 and 490 nm, monitored using an inverted microscope equipped with a Cascade 512B camera (Roper Scientific). The ratiometric recording of the emitted fluorescence was performed using the MetaMorph software.

Statistical analysis

Data are presented as the mean±standard deviation and analyzed using GraphPad Prism 7.0 (GraphPad Software Inc., San Diego, CA, USA). Differences between two groups were analyzed using Student's *t*-test and those among multiple groups using one-way analysis of variance (ANOVA) followed by Bonferroni's test. *P* values <0.05 were considered to indicate statistical significance.

RESULTS

MAM formation and high PDZD8 expression are observed in the pancreatic islets of HFD-induced diabetic mice

Compared with the NCD group, HFD dramatically increased fasting glucose levels (Supplementary Fig. 1A), decreased insulin levels (Supplementary Fig. 1C), and led to the development of insulin resistance (Supplementary Fig. 1B), indicating the DM mouse model was successfully established. Transmission electron microscopy (TEM) was used to observe and measure MAM formation in β-cells. The perimeter of MAM in the HFD model group was longer than that in the NCD group (Supplementary Fig. 1D and E). PDZD8 was highly expressed in the islet tissues of the HFD group compared with its expression in the NCD group (Supplementary Fig. 1F-H). MAM-related proteins in MAM, including IP3R1, GRP75, and VDAC1, were highly expressed in the HFD group compared with the NCD group (Supplementary Fig. 1H). These data demonstrate MAM formation and high PDZD8 expression in the DM mouse model.

AAV9 delivery of shPDZD8 inhibits MAM formation in the pancreatic islets of diabetic mice

The AAV9-shPDZD8 group exhibited lower fasting glucose levels and higher insulin levels than the AAV9-shNC group (Fig. 1A and C). Different to the effect of AAV9-shNC, AAV9-shPDZD8 significantly reversed HFD-induced insulin resistance (Fig. 1B). MAM perimeter was lengthened in the HFD group compared with that in the NCD group. Compared with the AAV9-shNC group, the AAV9-shPDZD8 shortened MAM perimeter (Fig. 1D and F). Compared with the NCD group, elevated VDAC1–IP3R1 signal counts appeared in the pancreatic islets of the HFD group. Compared with the AAV9-shNC group, AAV9-shPDZD8 suppressed VDAC1–IP3R1 staining intensity (Fig. 1E and G). The expression of IP3R1, GRP75, and VDAC1 in the HFD group was higher in the HFD group than in the NCD group. Compared with the AAV9-shNC group, the AAV9-shPDZD8 inhibited the expression of these proteins (Fig. 1H).

AAV9 delivery of shPDZD8 inhibits mitochondrial dysfunction and pancreatic β-cell death in diabetic mice

Compared with the NCD group, the levels of H_2O_2 and 4-hydroxynonenal (HNE) in the HFD group increased, while the

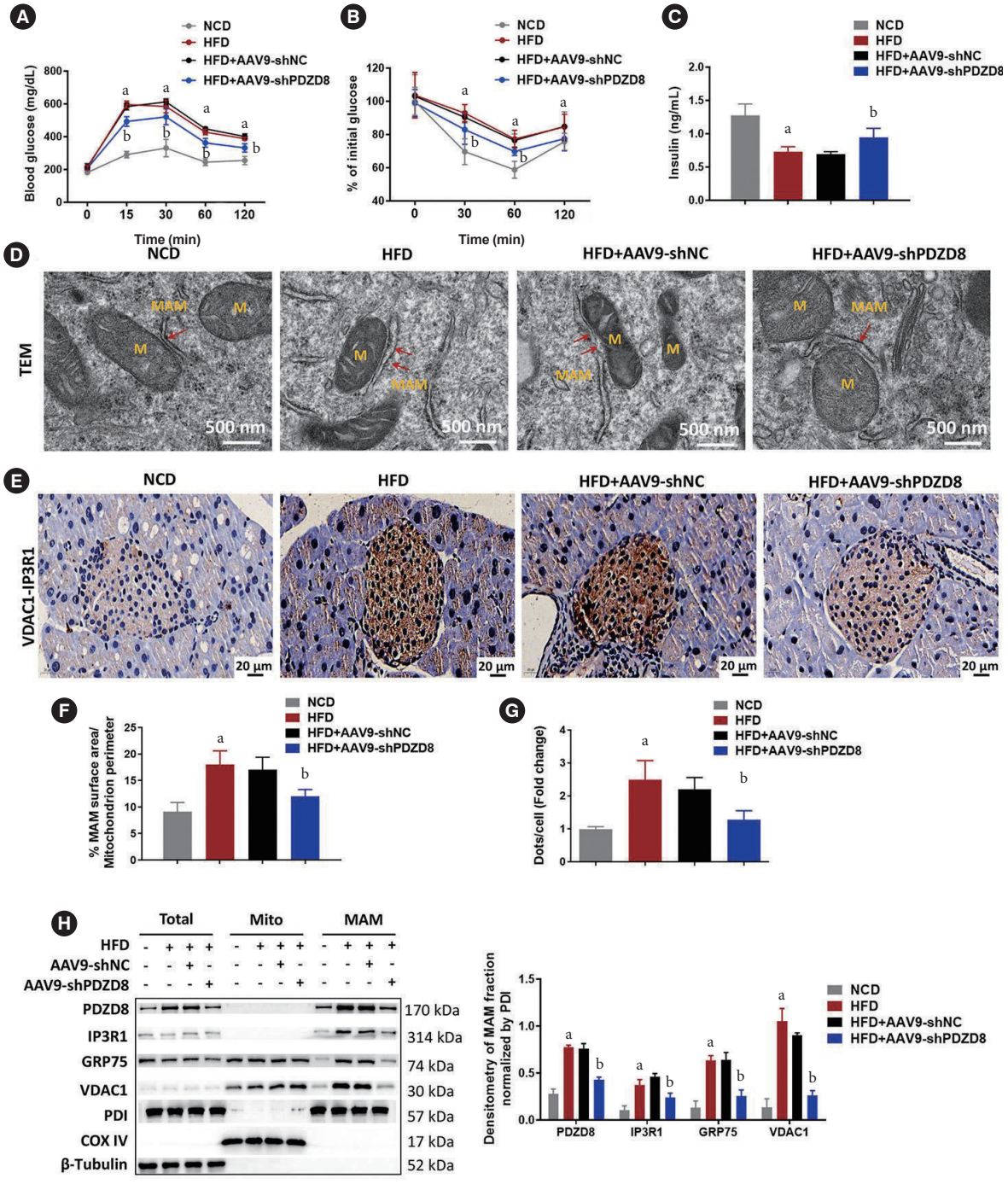

Fig. 1. Adeno-associated virus 9 (AAV9) delivery of short hairpin PDZ domain-containing 8 (shPDZD8) inhibits mitochondria-associated endoplasmic reticulum (ER) membrane (MAM) formation in the pancreatic islets of diabetic mice. (A) The blood-glucose level, (B) the fasting blood-glucose, and (C) the insulin level in mice. (D, F) The MAM in β-cells was measured using the transmission electron microscopy (TEM). The red arrows point to MAM. (E, G) The interaction between voltage-dependent anion-selective channel 1 (VDAC1) and inositol 1,4,5-triphosphate receptor type 1 (IP3R1) was detected using the proximity ligation assay (PLA). The dots represent the complex of VDAC1 and IP3R1. (H) The protein expression of MAM-related proteins in islet tissues was detected by Western blotting. M, mitochondria; GRP75, glucose-regulated protein 75; PDI, protein disulfide isomerase; COX IV, cytochrome c oxidase 4. [a]$P<0.05$ vs. normocaloric diet (NCD) group, [b]$P<0.05$ vs. high-fat diet (HFD)+AAV9-shRNA negative control (shNC) group.

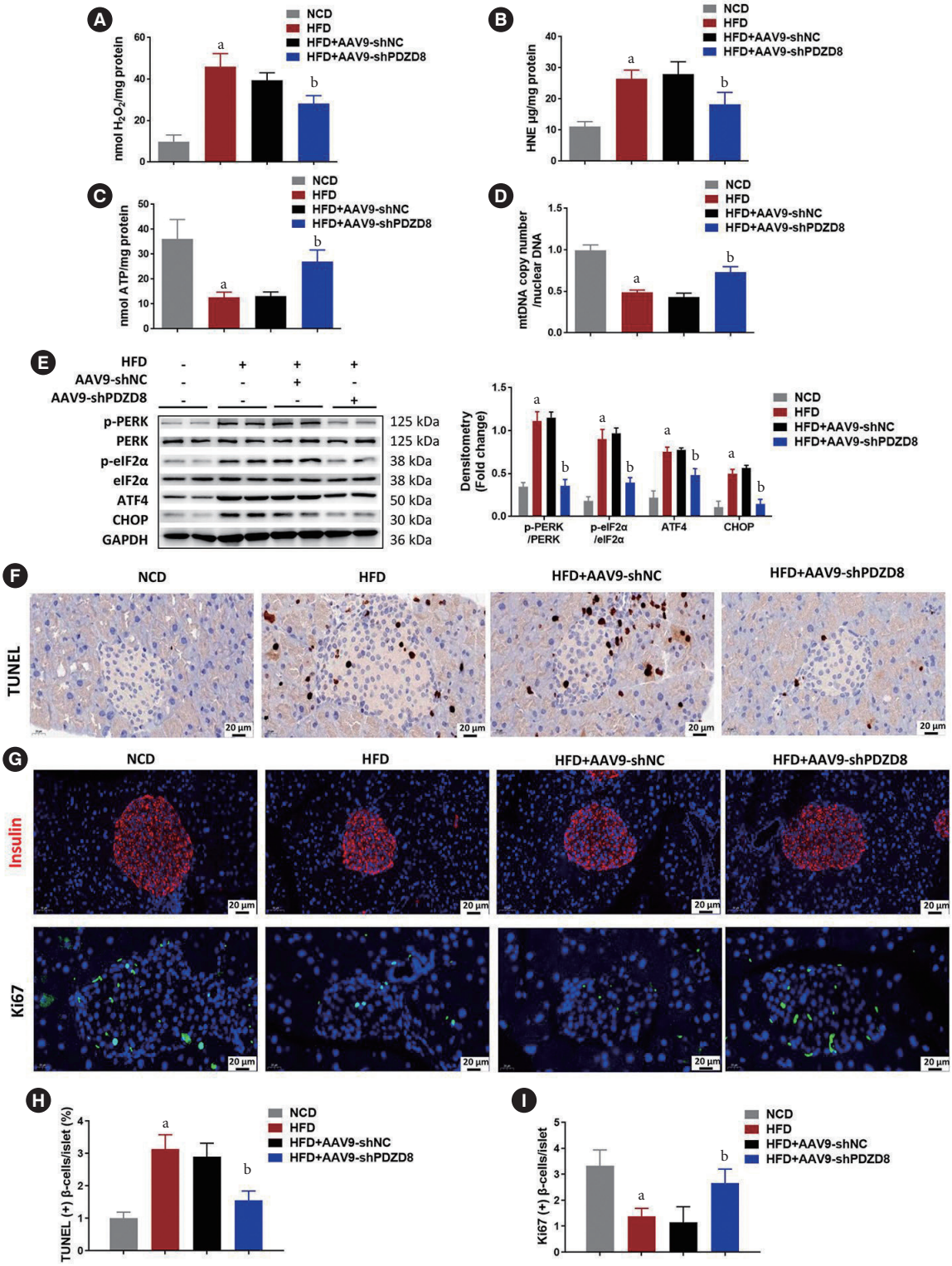

Fig. 2. Adeno-associated virus 9 (AAV9) delivery of short hairpin PDZ domain-containing 8 (shPDZD8) inhibits mitochondrial dysfunction and pancreatic β-cell death of diabetic mice. The levels of (A) H_2O_2, (B) 4-hydroxynonenal (HNE), (C) adenosine triphosphate (ATP), and (D) mitochondrial DNA (mtDNA) were measured using corresponding kits or quantitative real-time poly-

(*Continued to the next page*)

Fig. 2. Continued

merase chain reaction. (E) The expression of endoplasmic reticulum (ER) stress-related proteins were detected by Western blotting. (F) The apoptosis of β-cells in islet tissues was detected by terminal deoxynucleotidyl transferase dUTP nick end labeling (TUNEL) staining. (G) Immunofluorescence of insulin Ki67 was performed for detecting pancreatic β-cell mass and proliferation. (H) Quantitative data of TUNEL-positive β-cells per islet. (I) Quantitative data of Ki67-positive β-cells per islet. p-PERK, phosphorylated protein kinase R (PKR)-like endoplasmic reticulum kinase; p-eIF2α, phosphorylated eukaryotic translation initiation factor 2A; ATF4, activating transcription factor 4; CHOP, C/EBP-homologous protein; GAPDH, glyceraldehyde 3-phosphate dehydrogenase. [a]$P<0.05$ vs. normocaloric diet (NCD) group, [b]$P<0.05$ vs. high-fat diet (HFD)+AAV9-shRNA negative control (shNC) group.

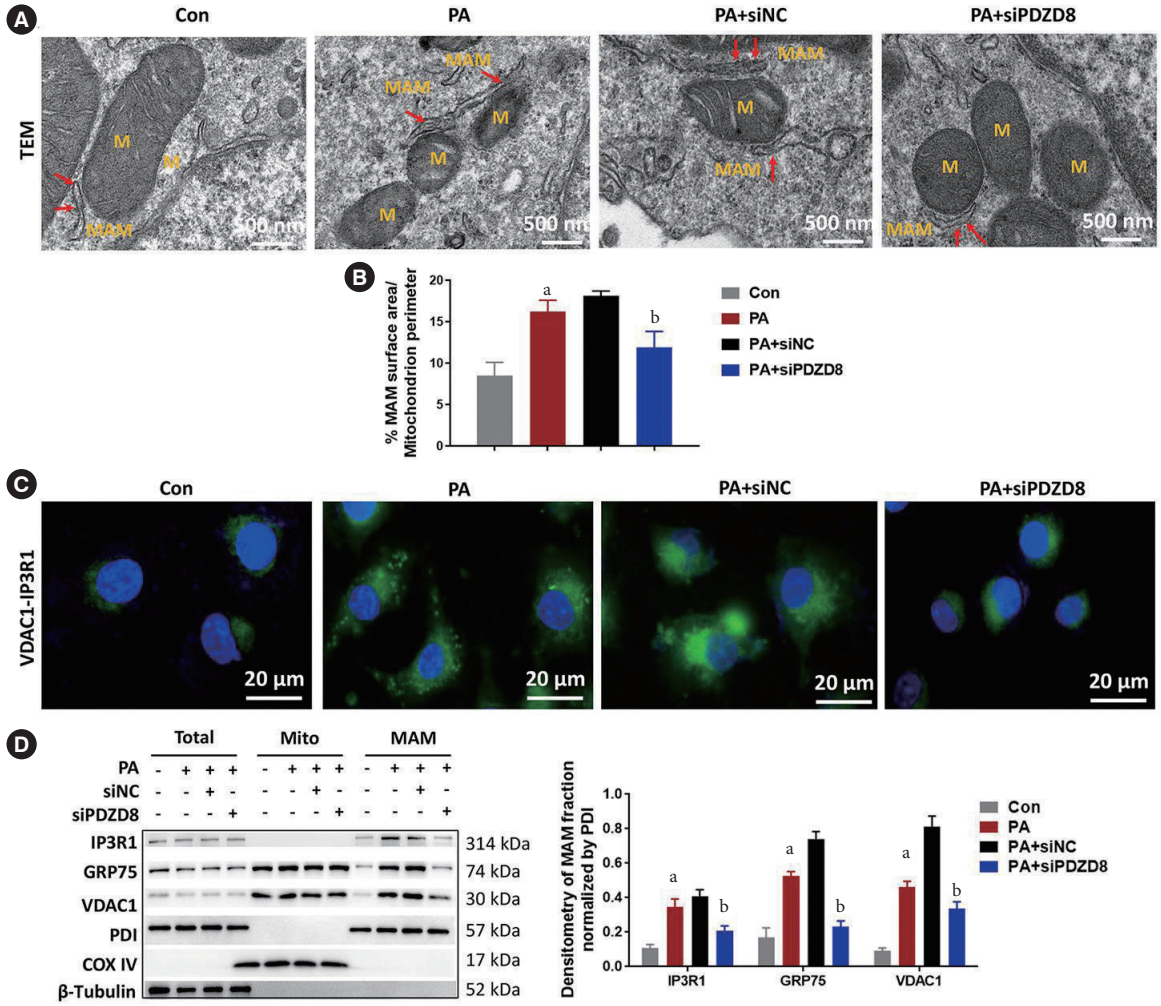

Fig. 3. PDZ domain-containing 8 (PDZD8) knockdown inhibits palmitic acid (PA)-induced mitochondria-associated endoplasmic reticulum membrane (MAM) formation in insulin 1 (INS-1) cells. (A, B) The MAM in INS-1 cells was measured using the transmission electron microscopy (TEM). The red arrows point to MAM. (C) The interaction between voltage-dependent anion-selective channel 1 (VDAC1) and inositol 1,4,5-triphosphate receptor type 1 (IP3R1) was detected using the proximity ligation assay. (D) The protein expression of PDZD8 and MAM-related proteins in INS-1 cells were detected by Western blotting. M, mitochondria; siPDZD8, siRNA PDZ domain-containing 8; GRP75, glucose-regulated protein 75; PDI, protein disulfide isomerase; COX IV, cytochrome c oxidase 4. [a]$P<0.05$ vs. control (Con) group, [b]$P<0.05$ vs. PA+shRNA negative control (shNC) group.

content of ATP and mtDNA decreased, indicating impaired mitochondrial function. Compared with AAV9-shNC, the AAV9-shPDZD8 alleviated the above effects (Fig. 2A-D). The levels of ER stress-related proteins in the islet tissues of the

HFD group remarkably increased compared with those of the NCD group. Compared with the AAV9-shNC group, AAV9-shPDZD8 alleviated the above condition (Fig. 2E). Compared with the NCD group, the percentage of TUNEL-positive β-cells increased in the HFD group, while AAV9-shPDZD8 reduced the percentage of TUNEL-positive β-cells (Fig. 2F and H). Additionally, pancreatic β-cell mass and proliferation were decreased in HFD group while AAV9-shPDZD8 increased them (Fig. 2G and I).

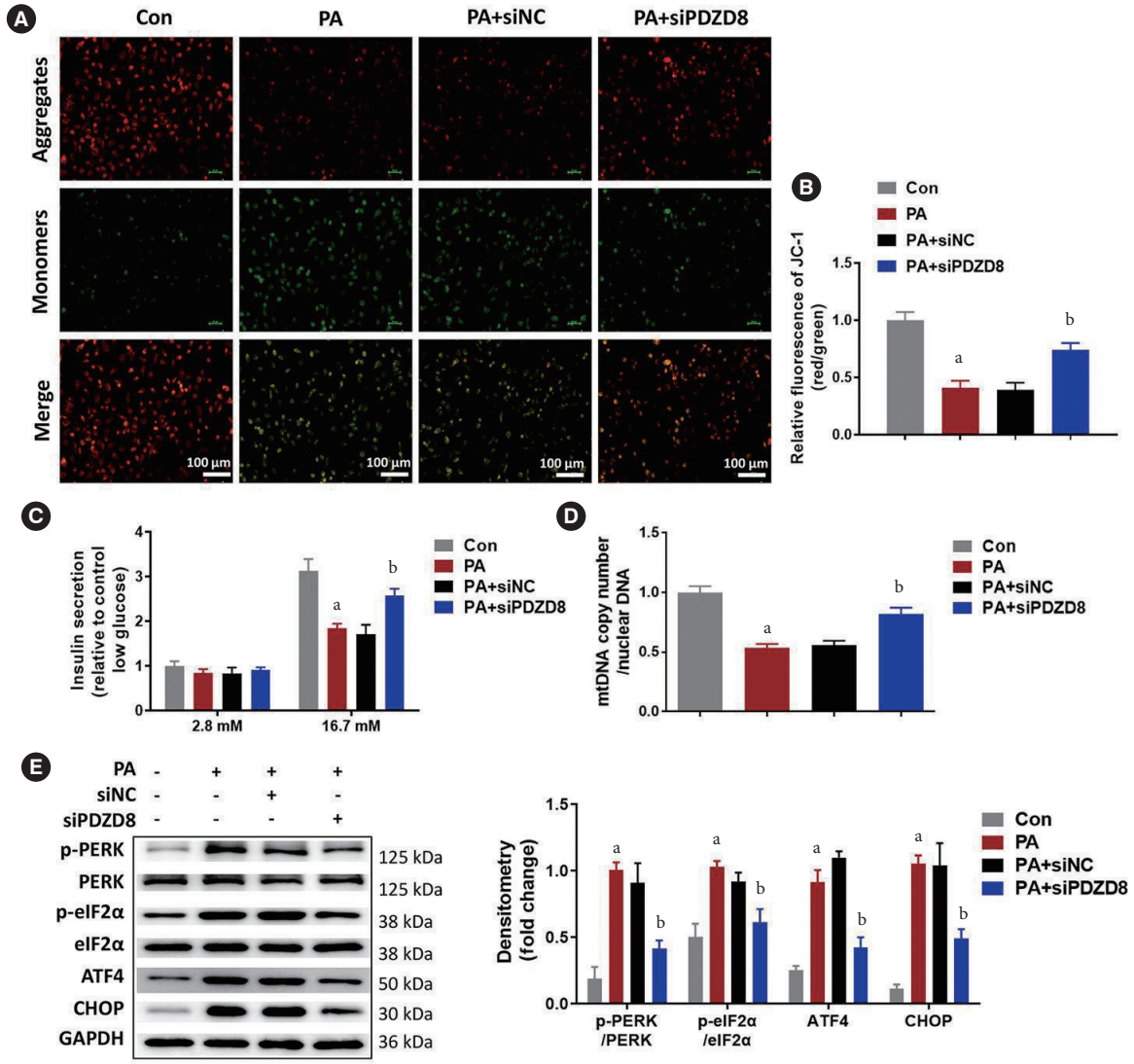

Fig. 4. PDZ domain-containing 8 (PDZD8) knockdown inhibits palmitic acid (PA)-induced mitochondrial dysfunction and endoplasmic reticulum (ER) stress in insulin 1 (INS-1) cells. (A, B) The mitochondrial membrane potential was detected using JC-1 probe. Green fluorescence indicates low mitochondrial membrane potential and red fluorescence indicates high mitochondrial membrane potential. (C) Insulin secretion was detected by enzyme-linked immunosorbent assay (ELISA) induced by 16.7 mM glucose as glucose-stimulated insulin secretion. (D) The copy fold of mitochondrial DNA (mtDNA). (E) The expression of ER stress-related proteins was detected by Western blotting. siPDZD8, siRNA PDZ domain-containing 8; p-PERK, phosphorylated protein kinase R (PKR)-like endoplasmic reticulum kinase; p-eIF2α, phosphorylated eukaryotic translation initiation factor 2A; ATF4, activating transcription factor 4; CHOP, C/EBP-homologous protein; GAPDH, glyceraldehyde 3-phosphate dehydrogenase. [a]$P<0.05$ vs. control (Con) group, [b]$P<0.05$ vs. PA+shRNA negative control (shNC) group.

PA increases MAM formation and PDZD8 expression in INS-1 cells

In vitro, PA promoted the formation of MAM in INS-1 cells. The perimeter of the MAM in the PA group was longer than that in the control group (Supplementary Fig. 2A and B). Compared with the control group, the PA group showed increased VDAC1–IP3R1 interactions in cells (Supplementary Fig. 2C). The expression of PDZD8 and MAM-related proteins, including IP3R1, GRP75, and VDAC1, in MAM dramatically increased in the PA group compared with that in the control group (Supplementary Fig. 2D).

PDZD8 knockdown inhibits PA-induced MAM formation in INS-1 cells

PA markedly lengthened the perimeter of MAM. PDZD8 knockdown shortened the perimeter of MAM in comparison with that in the siNC group (Fig. 3A and B). PA promoted the interaction between VDAC1 and IP3R1 in INS-1 cells. PDZD8 knockdown suppressed the interaction between VDAC1 and IP3R1 (Fig. 3C). Additionally, PA dramatically increased the expression of MAM-related proteins, including IP3R1, GRP75, and VDAC1, compared with that in the control group. PDZD8 knockdown significantly decreased the levels of these proteins (Fig. 3D).

PDZD8 knockdown inhibits PA-induced mitochondrial dysfunction and ER stress in INS-1 cells

PA decreased the relative fluorescence intensity of aggregate JC-1 compared with that in the control group. siPDZD8 transfection increased the relative fluorescence intensity of aggregate JC-1 compared with the effect in the siNC-transfected cells

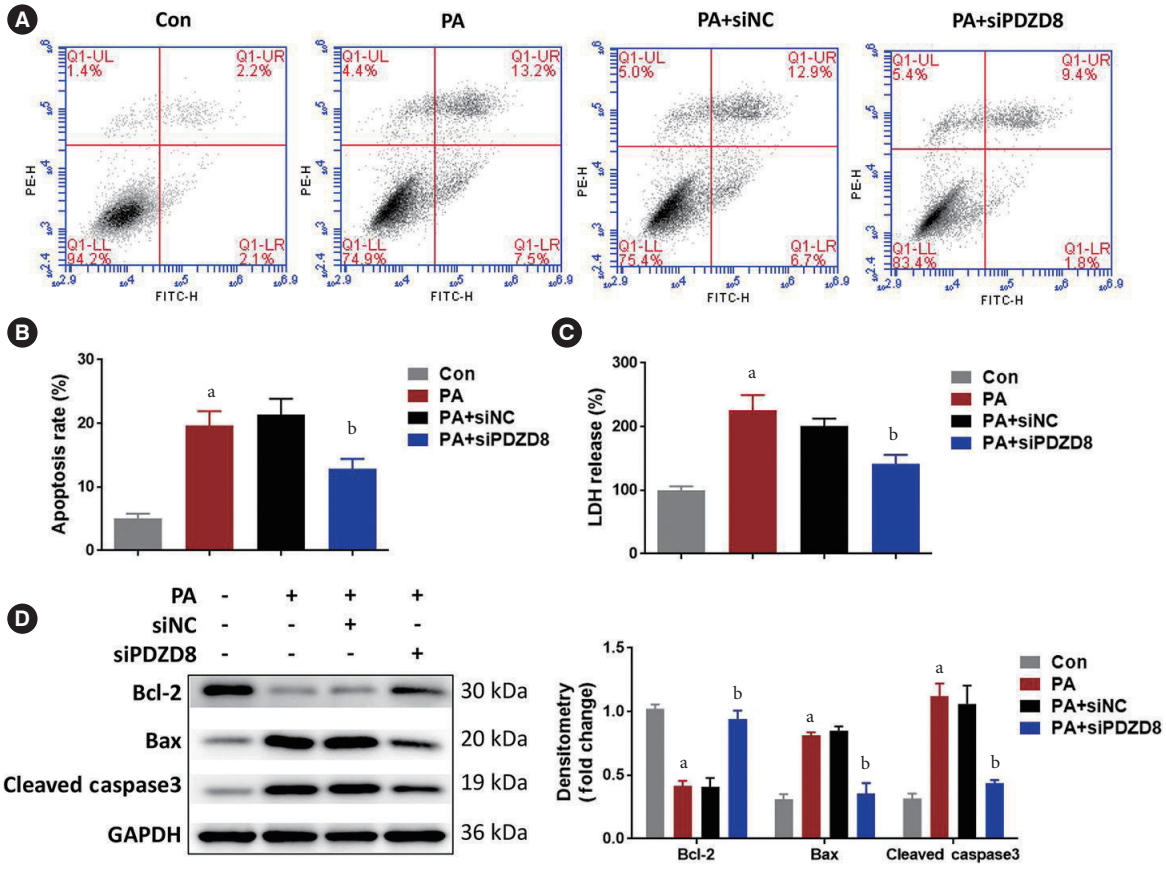

Fig. 5. PDZ domain-containing 8 (PDZD8) knockdown inhibits palmitic acid (PA)-induced insulin 1 (INS-1) cell death. (A, B) The apoptosis of INS-1 cells was detected using the flow cytometry. (C) The cytotoxicity was detected by lactate dehydrogenase (LDH) kit. (D) The expression of mitochondrial apoptosis-related proteins was detected by Western blotting. PE-H, phycoerythrin-H; FITC-H, fluorescein isothiocyanate-H; siPDZD8, siRNA PDZ domain-containing 8; Bcl-2, B cell lymphoma 2; Bax, BCL2 associated X, apoptosis regulator; GAPDH, glyceraldehyde 3-phosphate dehydrogenase. [a]$P<0.05$ vs. control (Con) group, [b]$P<0.05$ vs. PA+shRNA negative control (shNC) group.

(Fig. 4A and B). Considering that mitochondrial function is pivotal for insulin secretion, we examined the effects of PDZD8 silencing on glucose-stimulated insulin secretion (GSIS). PA decreased GSIS in INS-1 cells while PDZD8 silencing increased GSIS (Fig. 4C). PA reduced mtDNA copy numbers while PDZD8 silencing increased it (Fig. 4D). Higher levels of p-PERK/PERK, p-eIF2α/eIF2α, ATF4, and CHOP were observed in PA group than that in the control group. Compared with the siNC group, PDZD8 silencing alleviated the increased levels of these proteins (Fig. 4E).

PDZD8 knockdown inhibits PA-induced INS-1 cell death

Compared with the control group, PA increased the proportion of apoptotic cells. PDZD8 silencing reduced the proportion of apoptotic cells compared to the siNC group (Fig. 5A and B). PA increased the level of LDH, while PDZD8 silencing significant-

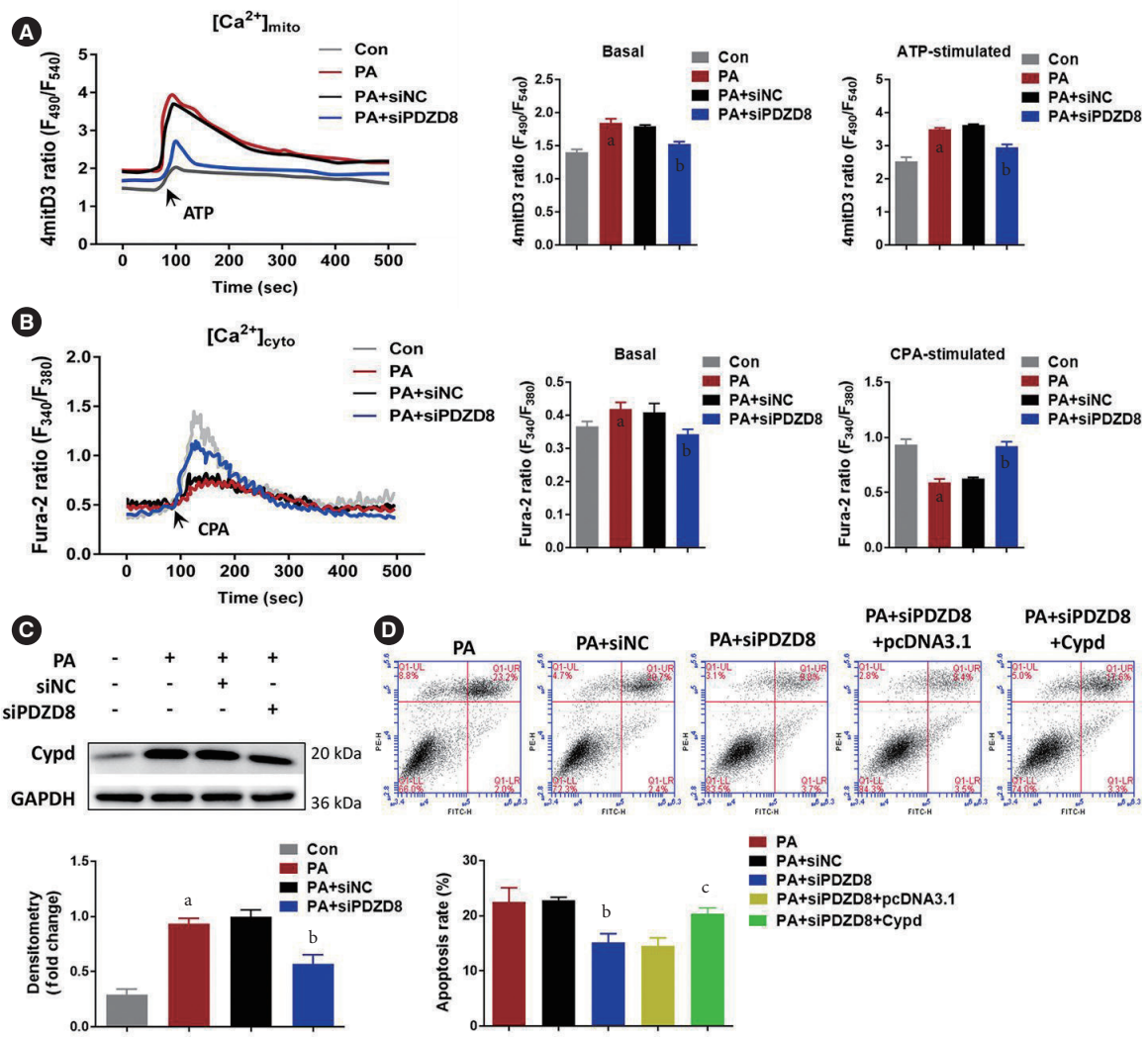

Fig. 6. PDZ domain-containing 8 (PDZD8) regulates insulin 1 (INS-1) cell death due to endoplasmic reticulum (ER)-mitochondria Ca^{2+} transfer and cyclophilin D (Cypd)-dependent mitochondrial permeability transition pore (mPTP) opening. (A, B) The subcellular localization of intracellular Ca^{2+} was detected using fluorescence probes. (C) The Cypd expression in INS-1 cells was detected by Western blotting. (D) The apoptosis of INS-1 cells was detected using the flow cytometry. ATP, adenosine triphosphate; CPA, cyclopiazonic acid; GAPDH, glyceraldehyde 3-phosphate dehydrogenase. [a]$P<0.05$ vs. control (Con) group, [b]$P<0.05$ vs. palmitic acid (PA)+shRNA negative control (shNC) group, [c]$P<0.05$ vs. PA+siRNA PDZ domain-containing 8 (siPDZD8)+pcDNA3.1 group.

ly inhibited LDH level (Fig. 5C). Compared with the control group, PA suppressed the level of Bcl-2 and increased the levels of Bax and cleaved caspase3. Compared with the siNC group, PDZD8 silencing alleviated the changes in the levels of these proteins (Fig. 5D).

PDZD8 regulates INS-1 cell death due to ER-mitochondria Ca^{2+} transfer and Cypd-dependent mitochondrial permeability transition pore opening

The levels of Ca^{2+} in the mitochondria and cytoplasm of cells in the PA group increased compared to those in the control group. After ATP and cyclopiazonic acid (CPA; a sarcoplasmic [SR]/ER Ca^{2+}-ATPase inhibitor) stimulation, Ca^{2+} levels in the mitochondria continued to increase, while those in the cytoplasm began to decrease, suggesting that PA promoted Ca^{2+} flow into the mitochondria. Compared with the siNC group, PDZD8 silencing alleviated the flow of Ca^{2+} into mitochondria (Fig. 6A and B). Cypd is a key regulatory protein for mitochondrial permeability transition pore (mPTP) opening that is closely related to Ca^{2+} kinetics. Cypd expression was determined to further reveal the mechanism by which PDZD8 affects pancreatic β-cell activity. PA promoted Cypd expression compared to the control group. However, siPDZD8 transfection inhibited Cypd expression (Fig. 6C). To further investigate the role of Cypd expression in PDZD8-mediated pancreatic β-cell apoptosis, PDZD8 siRNA and Cypd overexpression vectors were co-transfected into cells. Cypd overexpression alleviated the promoting effect of PDZD8 siRNA on cell apoptosis (Fig. 6D).

DISCUSSION

In this study, mice were fed HFD and injected with STZ to establish the T2DM mouse model. PDZD8 was highly expressed in the HFD mice. After PDZD8 knockdown in the HFD mice, the MAM perimeter, ER stress, mitochondria dysfunction, and pancreatic β-cell apoptosis were reduced, whereas pancreatic β-cell proliferation and mass were increased suggesting PDZD8 may be a new target for the treatment of T2DM by regulating the ER-mitochondria contact and Ca^{2+} dynamics (Supplementary Fig. 3).

ER stress is an important pathway for the transmission of apoptotic signals [23]. In response to various stimuli, ER dysfunction leads to the accumulation of misfolded proteins, ultimately resulting in ER stress [24]. PERK, a transmembrane signal transducer located in ER, is activated in response to ER stress [25]. Activated PERK (p-PERK) phosphorylates eIF2α and activates the selective translation of ATF4 [26]. Next, the continuous expression of ATF4 promotes the expression of apoptosis-related genes under strong ER stress. CHOP, a gene downstream of ATF4, is a transcription factor that promotes apoptosis [27]. In this study, the levels of ER stress-related proteins in the islet tissues of HFD mice and PA-treated pancreatic β-cells were dramatically up-regulated, while PDZD8 knockdown remarkably inhibited ER stress.

The mitochondria play a key role in the regulation of metabolic pathways and in maintaining a proper energy balance in tissues [28,29]. Most cellular ATP is produced through the tricarboxylic acid cycle and oxidative phosphorylation to meet cell energy requirements [30]. mtDNA carries the genetic material in mitochondria [31]. Mitochondrial dysfunction can lead to ultrastructural mitochondrial damage, ATP depletion, increased permeability of outer and inner membranes, reactive oxygen species (ROS) overproduction, and mtDNA deletion [32,33]. DM is associated with decreased mitochondrial function, including decreased mitochondrial numbers [34], impaired lipid oxidation [35,36], excessive production of ROS [34,37], and mtDNA defects and mutations [38,39]. HNE is considered to be a cytotoxic product of lipid peroxidation [40]. In this study, the H_2O_2 and HNE levels increased, while the ATP content and mtDNA copy number decreased in HFD mice. The mitochondrial membrane potential and mtDNA copy number of PA-treated pancreatic β-cells markedly decreased. PDZD8 knockdown inhibited the levels of H_2O_2 and HNE and increased ATP content and mtDNA copy number in the pancreatic tissue of HFD mice. PDZD8 knockdown also increased the mitochondrial membrane potential and mtDNA copy number in PA-treated β-cells, suggesting PDZD8 knockdown can alleviate diabetic mitochondrial dysfunction.

MAM, a special domain that mediates the tight connections between mitochondria and ER, plays an important role in maintaining cellular homeostasis [41]. Impaired MAM signaling can lead to the onset or exacerbation of many diseases, including diabetes [41]. MAMs affect insulin signaling through pathways related to mitochondrial function, ER stress, calcium signaling, and lipid metabolism [42]. Various proteins, including IP3R1, VDAC1, and GRP75, are enriched at the MAM interface to maintain MAM structure and function [43]. MAM is a bridge for Ca^{2+} transfer between the ER and mitochondria [44]. Ca^{2+} is released from ER into the mitochondria via the MAM complex IP3R1–VDAC1 [45]. Shortening the distance

between MAMs leads to increased efficiency of Ca^{2+} transport, resulting in mitochondrial Ca^{2+} overload [44]. Excessive Ca^{2+} accumulation in the mitochondria opens mPTP and promotes the release of pro-apoptotic factors [46]. Cypd, a major regulator of mPTP, mediates this process [47]. In this study, PDZD8 knockdown remarkably shortened the MAM perimeter, decreased the expression of the MAM-related proteins IP3R1, VDAC1, and GRP75, and inhibited the interaction between VDAC1 and IP3R1, thus alleviating the flow of Ca^{2+} into the mitochondria. Furthermore, PDZD8 knockdown dramatically inhibited Cypd protein levels and reduced the death of PA-treated β-cells. These data suggest that PDZD8 knockdown may inhibit β-cell apoptosis by regulating Ca^{2+} kinetics through MAM.

Lipotoxicity and glucotoxicity are implicated in the pathogenesis of T2DM [48]. Lipotoxicity refers to cellular dysfunction induced by increased levels of circulating free fatty acids or cellular fat content. Glucotoxicity is defined as cellular damage induced by elevated blood-glucose concentration [49]. Both lipotoxicity and glucotoxicity manifest in the liver, muscles, and pancreatic islets. Excess free fatty acids, or glucose, or both may contribute to pancreatic β-cell death and the diabetic state. In this study, the effects of PDZD8 silencing on a PA-induced lipotoxicity model were investigated. The effects of PDZD8 silencing on glucotoxicity or glucolipotoxicity models should be studied in the future.

This study puts forth a new idea: in the progression of DM, PDZD8 can promote mitochondrial dysfunction by promoting MAM formation, increase the flow of Ca^{2+} into the mitochondria, and cause mitochondrial-related cell death of pancreatic β-cells, ultimately contributing to DM progression.

SUPPLEMENTARY MATERIALS

Supplementary materials related to this article can be found online at https://doi.org/10.4093/dmj.2023.0275.

CONFLICTS OF INTEREST

No potential conflict of interest relevant to this article was reported.

AUTHOR CONTRIBUTIONS

Conception or design: Y.L.
Acquisition, analysis, or interpretation of data: all authors.
Drafting the work or revising: all authors.
Final approval of the manuscript: all authors.

ORCID

Yongxin Liu *https://orcid.org/0009-0008-3556-8049*
Yongqing Wei *https://orcid.org/0000-0001-9123-1530*
Xiujuan Zhang *https://orcid.org/0009-0001-5959-7652*

FUNDING

This study was provided by the National Natural Science Foundation of China (No. 81970700).

ACKNOWLEDGMENTS

None

REFERENCES

1. Pang B, Li QW, Qin YL, Dong GT, Feng S, Wang J, et al. Traditional Chinese medicine for diabetic retinopathy: a systematic review and meta-analysis. Medicine (Baltimore) 2020;99:e19102.
2. Xu L, Li Y, Dai Y, Peng J. Natural products for the treatment of type 2 diabetes mellitus: pharmacology and mechanisms. Pharmacol Res 2018;130:451-65.
3. Tanase DM, Gosav EM, Neculae E, Costea CF, Ciocoiu M, Hurjui LL, et al. Role of gut microbiota on onset and progression of microvascular complications of type 2 diabetes (T2DM). Nutrients 2020;12:3719.
4. Inaishi J, Saisho Y. Beta-cell mass in obesity and type 2 diabetes, and its relation to pancreas fat: a mini-review. Nutrients 2020;12:3846.
5. Wang JJ, Park KS, Dhimal N, Shen S, Tang X, Qu J, et al. Proteomic analysis of retinal mitochondria-associated ER membranes identified novel proteins of retinal degeneration in long-term diabetes. Cells 2022;11:2819.
6. Zhang SX, Sanders E, Fliesler SJ, Wang JJ. Endoplasmic reticulum stress and the unfolded protein responses in retinal degeneration. Exp Eye Res 2014;125:30-40.
7. Huang C, Wang JJ, Jing G, Li J, Jin C, Yu Q, et al. Erp29 attenuates cigarette smoke extract-induced endoplasmic reticulum stress and mitigates tight junction damage in retinal pigment epithelial cells. Invest Ophthalmol Vis Sci 2015;56:6196-207.

8. Csordas G, Renken C, Varnai P, Walter L, Weaver D, Buttle KF, et al. Structural and functional features and significance of the physical linkage between ER and mitochondria. J Cell Biol 2006;174:915-21.
9. Lopez Gavilanez E, Johansson H, McCloskey E, Harvey NC, Segale Bajana A, Marriott Blum D, et al. Assessing the risk of osteoporotic fractures: the Ecuadorian FRAX model. Arch Osteoporos 2019;14:93.
10. Ma JH, Shen S, Wang JJ, He Z, Poon A, Li J, et al. Comparative proteomic analysis of the mitochondria-associated ER membrane (MAM) in a long-term type 2 diabetic rodent model. Sci Rep 2017;7:2062.
11. Schrader M, Godinho LF, Costello JL, Islinger M. The different facets of organelle interplay: an overview of organelle interactions. Front Cell Dev Biol 2015;3:56.
12. Betz C, Stracka D, Prescianotto-Baschong C, Frieden M, Demaurex N, Hall MN. Feature article: mTOR complex 2-Akt signaling at mitochondria-associated endoplasmic reticulum membranes (MAM) regulates mitochondrial physiology. Proc Natl Acad Sci U S A 2013;110:12526-34.
13. Bononi A, Bonora M, Marchi S, Missiroli S, Poletti F, Giorgi C, et al. Identification of PTEN at the ER and MAMs and its regulation of Ca(2+) signaling and apoptosis in a protein phosphatase-dependent manner. Cell Death Differ 2013;20:1631-43.
14. Hirabayashi Y, Kwon SK, Paek H, Pernice WM, Paul MA, Lee J, et al. ER-mitochondria tethering by PDZD8 regulates Ca2+ dynamics in mammalian neurons. Science 2017;358:623-30.
15. Jeyasimman D, Saheki Y. SMP domain proteins in membrane lipid dynamics. Biochim Biophys Acta Mol Cell Biol Lipids 2020;1865:158447.
16. Shirane M, Wada M, Morita K, Hayashi N, Kunimatsu R, Matsumoto Y, et al. Protrudin and PDZD8 contribute to neuronal integrity by promoting lipid extraction required for endosome maturation. Nat Commun 2020;11:4576.
17. Guillen-Samander A, Bian X, De Camilli P. PDZD8 mediates a Rab7-dependent interaction of the ER with late endosomes and lysosomes. Proc Natl Acad Sci U S A 2019;116:22619-23.
18. Khan H, Chen L, Tan L, Im YJ. Structural basis of human PDZD8-Rab7 interaction for the ER-late endosome tethering. Sci Rep 2021;11:18859.
19. Gao Y, Xiong J, Chu QZ, Ji WK. PDZD8-mediated lipid transfer at contacts between the ER and late endosomes/lysosomes is required for neurite outgrowth. J Cell Sci 2022;135:jcs255026.
20. Wei W, Wang C, Wang L, Zhang J. circ_0020123 promotes cell proliferation and migration in lung adenocarcinoma via PDZD8. Open Med (Wars) 2022;17:536-49.
21. Hojo Y, Kishi S, Mori S, Fujiwara-Tani R, Sasaki T, Fujii K, et al. Sunitinib and pterostilbene combination treatment exerts antitumor effects in gastric cancer via suppression of PDZD8. Int J Mol Sci 2022;23:4002.
22. Henning MS, Stiedl P, Barry DS, McMahon R, Morham SG, Walsh D, et al. PDZD8 is a novel moesin-interacting cytoskeletal regulatory protein that suppresses infection by herpes simplex virus type 1. Virology 2011;415:114-21.
23. Szegezdi E, Logue SE, Gorman AM, Samali A. Mediators of endoplasmic reticulum stress-induced apoptosis. EMBO Rep 2006;7:880-5.
24. Ron D, Walter P. Signal integration in the endoplasmic reticulum unfolded protein response. Nat Rev Mol Cell Biol 2007;8:519-29.
25. Malhotra JD, Kaufman RJ. Endoplasmic reticulum stress and oxidative stress: a vicious cycle or a double-edged sword? Antioxid Redox Signal 2007;9:2277-93.
26. Rozpedek W, Pytel D, Mucha B, Leszczynska H, Diehl JA, Majsterek I. The role of the PERK/eIF2α/ATF4/CHOP signaling pathway in tumor progression during endoplasmic reticulum stress. Curr Mol Med 2016;16:533-44.
27. Xu J, Zhou Q, Xu W, Cai L. Endoplasmic reticulum stress and diabetic cardiomyopathy. Exp Diabetes Res 2012;2012:827971.
28. Thivolet C, Vial G, Cassel R, Rieusset J, Madec AM. Reduction of endoplasmic reticulum-mitochondria interactions in beta cells from patients with type 2 diabetes. PLoS One 2017;12:e0182027.
29. Rovira-Llopis S, Banuls C, Diaz-Morales N, Hernandez-Mijares A, Rocha M, Victor VM. Mitochondrial dynamics in type 2 diabetes: pathophysiological implications. Redox Biol 2017;11:637-45.
30. Flemming N, Pernoud L, Forbes J, Gallo L. Mitochondrial dysfunction in individuals with diabetic kidney disease: a systematic review. Cells 2022;11:2481.
31. Yan C, Duanmu X, Zeng L, Liu B, Song Z. Mitochondrial DNA: distribution, mutations, and elimination. Cells 2019;8:379.
32. Wei Y, Rector RS, Thyfault JP, Ibdah JA. Nonalcoholic fatty liver disease and mitochondrial dysfunction. World J Gastroenterol 2008;14:193-9.
33. Li Z, Li Y, Zhang HX, Guo JR, Lam CW, Wang CY, et al. Mitochondria-mediated pathogenesis and therapeutics for non-alcoholic fatty liver disease. Mol Nutr Food Res 2019;63:e1900043.
34. Boushel R, Gnaiger E, Schjerling P, Skovbro M, Kraunsoe R, Dela F. Patients with type 2 diabetes have normal mitochondri-

al function in skeletal muscle. Diabetologia 2007;50:790-6.
35. Patti ME, Butte AJ, Crunkhorn S, Cusi K, Berria R, Kashyap S, et al. Coordinated reduction of genes of oxidative metabolism in humans with insulin resistance and diabetes: potential role of PGC1 and NRF1. Proc Natl Acad Sci U S A 2003;100:8466-71.
36. Vamecq J, Dessein AF, Fontaine M, Briand G, Porchet N, Latruffe N, et al. Mitochondrial dysfunction and lipid homeostasis. Curr Drug Metab 2012;13:1388-400.
37. Nishikawa T, Kukidome D, Sonoda K, Fujisawa K, Matsuhisa T, Motoshima H, et al. Impact of mitochondrial ROS production in the pathogenesis of insulin resistance. Diabetes Res Clin Pract 2007;77 Suppl 1:S161-4.
38. Molnar MJ, Kovacs GG. Mitochondrial diseases. Handb Clin Neurol 2017;145:147-55.
39. Fex M, Nicholas LM, Vishnu N, Medina A, Sharoyko VV, Nicholls DG, et al. The pathogenetic role of β-cell mitochondria in type 2 diabetes. J Endocrinol 2018;236:R145-59.
40. Zarkovic N. 4-Hydroxynonenal as a bioactive marker of pathophysiological processes. Mol Aspects Med 2003;24:281-91.
41. Xu H, Zhou W, Zhan L, Bi T, Lu X. Liver mitochondria-associated endoplasmic reticulum membrane proteomics for studying the effects of ZiBuPiYin recipe on Zucker diabetic fatty rats after chronic psychological stress. Front Cell Dev Biol 2022;10:995732.
42. Cheng H, Gang X, He G, Liu Y, Wang Y, Zhao X, et al. The molecular mechanisms underlying mitochondria-associated endoplasmic reticulum membrane-induced insulin resistance. Front Endocrinol (Lausanne) 2020;11:592129.
43. Lee S, Min KT. The interface between ER and mitochondria: molecular compositions and functions. Mol Cells 2018;41:1000-7.
44. Yang S, Zhou R, Zhang C, He S, Su Z. Mitochondria-associated endoplasmic reticulum membranes in the pathogenesis of type 2 diabetes mellitus. Front Cell Dev Biol 2020;8:571554.
45. D'Eletto M, Rossin F, Occhigrossi L, Farrace MG, Faccenda D, Desai R, et al. Transglutaminase type 2 regulates ER-mitochondria contact sites by interacting with GRP75. Cell Rep 2018;25:3573-81.
46. Rizzuto R, De Stefani D, Raffaello A, Mammucari C. Mitochondria as sensors and regulators of calcium signalling. Nat Rev Mol Cell Biol 2012;13:566-78.
47. Fayaz SM, Raj YV, Krishnamurthy RG. CypD: the key to the death door. CNS Neurol Disord Drug Targets 2015;14:654-63.
48. Poitout V, Robertson RP. Glucolipotoxicity: fuel excess and beta-cell dysfunction. Endocr Rev 2008;29:351-66.
49. Sivitz WI. Lipotoxicity and glucotoxicity in type 2 diabetes: effects on development and progression. Postgrad Med 2001;109:55-64.